



HAL
open science

Incorporation and localisation of alkanes in a protomembrane model

Loreto Misuraca, Josephine Loricco, Philippe Oger, Judith Peters, Bruno Demé

► **To cite this version:**

Loreto Misuraca, Josephine Loricco, Philippe Oger, Judith Peters, Bruno Demé. Incorporation and localisation of alkanes in a protomembrane model. *Biochimica et Biophysica Acta: Biomembranes*, 2023, 1865 (3), pp.184119. 10.1016/j.bbamem.2023.184119. hal-04297309

HAL Id: hal-04297309

<https://hal.science/hal-04297309>

Submitted on 21 Nov 2023

HAL is a multi-disciplinary open access archive for the deposit and dissemination of scientific research documents, whether they are published or not. The documents may come from teaching and research institutions in France or abroad, or from public or private research centers.

L'archive ouverte pluridisciplinaire **HAL**, est destinée au dépôt et à la diffusion de documents scientifiques de niveau recherche, publiés ou non, émanant des établissements d'enseignement et de recherche français ou étrangers, des laboratoires publics ou privés.

Alkane localisation inside a compliant protomembrane model

Loreto Misuraca^{a,b}, Josephine LoRicco^c, Philippe Oger^c, Judith Peters^{a,b,d,*}, Bruno Demé^{b,*}

^a Univ. Grenoble Alpes, CNRS, LIPhy, 38000 Grenoble, France.

^b Institut Laue Langevin, F-38042 Grenoble Cedex 9, France

^c INSA Lyon, Université de Lyon, CNRS, UMR5240, Villeurbanne, France.

^d Institut Universitaire de France.

*Corresponding authors : Judith Peters, jpeters@ill.fr and Bruno Demé, deme@ill.fr

Abstract

Protomembranes at the origin of life were likely composed of short-chain lipids, readily available on the early Earth. On the other hand, membranes formed by such lipids are less stable and more permeable under extreme conditions, so that a novel membrane architecture was suggested to validate the accuracy of this assumption. The model membrane includes the presence of a layer of alkanes in the mid-plane of the protomembrane in between the two monolayer leaflets and lying perpendicular to the lipid acyl chains. Here, we investigated such possibility experimentally for membranes formed by the short-chain phospholipid 1,2-didecanoyl-*sn*-glycero-3-phosphocholine, including or not the alkanes eicosane, squalane or triacontane by means of neutron membrane diffraction and contrast variation. We found strong indications for an incorporation of two of the three alkanes in the membrane mid-plane through the determination of neutron scattering length density profiles and the membrane swelling at various relative humidities indicating a slightly increased bilayer thickness when the alkanes are incorporated into the bilayers. The selectivity of the incorporation points out the role of the length of the n-alkanes with respect to the capacity of the membrane to incorporate them.

Introduction

The cell membrane is among the most fascinating macromolecular structures that make up all living systems. It is a biological, mainly two-dimensional matrix that separates and protects the interior of the cell from its environment. The basic unit of cell membranes (which generally consist of lipids, proteins and carbohydrates) is a bilayer of polar lipids (phospholipids, glycolipids) whose polar head-groups point outwards and stabilize the bilayer, while the hydrophobic acyl chains constitute the membrane core. Biomembranes promote the compartmentalization of living systems, which is an essential property for the definition of life. This fact probably played a key role in the early stages of the formation of the first membranes and thus in the origin of life on our planet [1-5].

Several structural studies have been performed on lipid membranes to obtain quantitative information on their molecular organization, phase transitions and phase separations, incorporation and effects of host molecules and macromolecules [6], etc. These structural characterizations are often complicated by the fact that the biologically relevant phases are not crystalline, therefore there is no three-dimensional repeat unit that can be resolved through usual crystallographic methods. Instead, lipids typically arrange into liquid-crystalline phases, e.g. gel (L_{β} , P_{β}) or fluid (L_{α}) lamellar phases, which possess intrinsic static and/or dynamic lateral disorder. X-ray and neutron diffraction techniques have been important tools in this respect, because they allow one-dimensional information of the membrane ordering to

48 be obtained both in the bilayer plane and perpendicular to it, despite the lateral disorder of
49 the various lamellar phases precisely when in the biologically relevant (L_{α}) fluid phase.

50 From seminal studies performed back in the 1970s [7-10], a methodology was developed to
51 extract the neutron and x-ray scattering length density (SLD) profiles of membranes from
52 solid-supported stacks of parallel membranes opening the field known today as *membrane*
53 *diffraction*. The analysis of the SLD profiles gives information on the average positioning and
54 dimensions of each membrane constituent [11]: hydrocarbon chains, headgroup components
55 (e.g. the phosphate and the choline groups) [12, 13], water and additional incorporated host
56 molecules, when present (e.g. cholesterol) [8, 9].

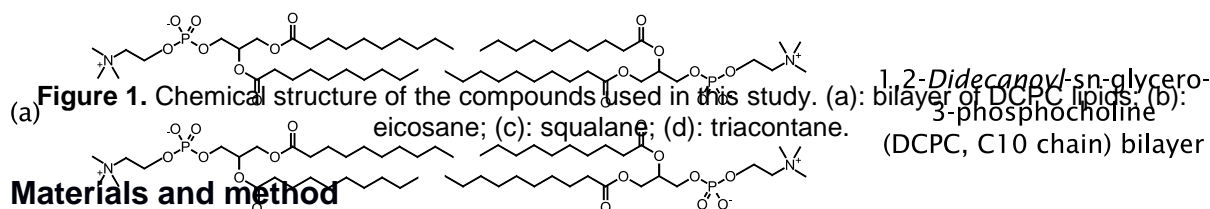
57 With this quantitative information at hand, one can investigate the location of intercalants
58 within the membrane and correlate it with the observed consequences on the membrane
59 structure, as well as its properties and functioning. This was done, for example, by using n-
60 alkanes of varying chain length to investigate the mechanisms of anaesthesia [14, 15]. These
61 studies proved that a significant amount of n-alkanes (e.g. hexane [16]) entered the bilayer
62 core, although the resolution was not sufficient to determine whether there was a preferential
63 positioning (i.e. sitting parallel or perpendicular to the lipid acyl chains). Another study [17]
64 was performed using high amounts of C6 – C16 n-alkanes (0.3 – 0.9 alkane:lipid ratio) on
65 egg PC membranes, finding that smaller n-alkane chain lengths contributed to an increase in
66 bilayer thickness. More recently, the exact positioning of small amounts of squalane
67 (branched C30 alkane) was determined in model membranes made of DOPC:DOPG [18]
68 and an archaea-mimicking mixture DOPhPC:DOPhPE [19]. In both cases, squalane was
69 found to enter the lipid membrane and to position in the mid-plane of the bilayers
70 perpendicularly to the lipid tails. Such novel membrane architecture was suggested earlier
71 by Cario et al. [20] and then confirmed experimentally. Moreover, the two studies highlighted
72 the possibilities for the incorporated molecules to act as proton permeability barrier [18] and
73 to trigger domain formation [19].

74 In analogy with previous findings, our group has studied the incorporation of n-alkanes in
75 early life membrane models composed of short single chain amphiphiles (SCAs) with 10-
76 carbon (C10) chain length [21]. The reason for this lies in the likely presence of a broad size
77 distribution of n-alkanes (especially linear ones) along with SCAs in the early Earth
78 environment, as both species are readily formed via Fischer-Tropsch type reactions [22, 23].
79 If a structural role could be identified for such apolar molecules into the prebiotic
80 membranes, this would help explain how SCA membranes could have withstood the harsh
81 environmental conditions of the early planet. In our recent study [21], we found that the
82 alkanes squalane and eicosane (C20 linear) decrease the temperature induced membrane
83 swelling of multilamellar vesicles (MLVs) and decrease the membrane sensitivity at high
84 hydrostatic pressure. These results show that the incorporation of n-alkanes can indeed
85 confer a higher membrane stability at high temperatures and pressures and therefore could
86 have played a major role in the formation of the first forms of life.

87 It is now important to determine the actual positioning of such molecules inside short-chain
88 lipid membranes. First, the existence of a preferential orientation of the alkanes inside the
89 membrane could help gain insight into the mechanisms by which the bilayers acquire a
90 higher thermo- and piezo-stability. Second, it might explain the need for more or less
91 intercalant in order to obtain significant effects in the membrane (for instance, an orientation
92 of the alkanes perpendicular to the acyl chains might correlate with very small amounts
93 needed in the membrane). Third, the positioning may affect membrane structural features,
94 e.g. the bilayer thickness, possibly offering a way to obtain a thicker membrane even in
95 conditions where only short chain lipids are available.

96 Previous structural studies on model membranes have focused on lipids having chain length
 97 of 12 carbons or longer [12, 13, 24]. Here, we performed our investigation using the C10 PC
 98 lipid 1,2-didecanoyl-*sn*-glycero-3-phosphocholine (hereafter DCPC, Figure 1a) as
 99 phosphocholine C10 analogue of the previously studied SCA membranes [21, 25]. This
 100 allows to benefit from optimized procedures for successfully producing membrane stacks
 101 onto silicon substrates [12], which are needed for obtaining structural information by
 102 membrane diffraction. We combined two approaches to neutron diffraction studies, contrast
 103 variation and membrane swelling (see Materials and Methods section), to fully characterize
 104 DCPC bilayers in the absence or presence of small amounts of three alkanes: eicosane
 105 (Figure 1b), squalane (Figure 1c) and triacontane (C30 linear, Figure 1d).

106 We found that the alkanes eicosane and squalane enter the membrane hydrophobic core
 107 and lead to an increase of the bilayer thickness compared to the alkane-free sample.
 108 Conversely, the triacontane does not lead to an increase in membrane thickness, hence
 109 questioning its incorporation into the membrane and suggesting a role of the n-alkane length
 110 for a successful inclusion in the bilayer.



116 1. Sample preparation

117 DCPC was purchased from Avanti Polar Lipids (Alabaster, AL, USA). Hydrogenated and
 118 perdeuterated eicosane, squalane and triacontane were purchased from (b) (c) (d) Sigma
 119 (Merck, Darmstadt, Germany). All products were used as received from the manufacturer,
 120 without further purification. 5 mg of DCPC or DCPC with 4% molar of the corresponding
 121 hydrogenated or deuterated alkane (eicosane, squalane or triacontane) were dissolved in
 122 chloroform:methanol (2:1), spread on a silicon wafer (Si-Mat., Kaufering, Germany) using the
 123 "rock and roll" method [26] and dried overnight under vacuum. Next, (c) (d) the samples
 124 were placed in sealed Falcon tubes containing about 100 μL of H_2O at 40 $^\circ\text{C}$ for 24 hours of
 125 annealing. Finally, samples were stored at ambient temperature before the experiments.

126 2. Neutron Diffraction experiments

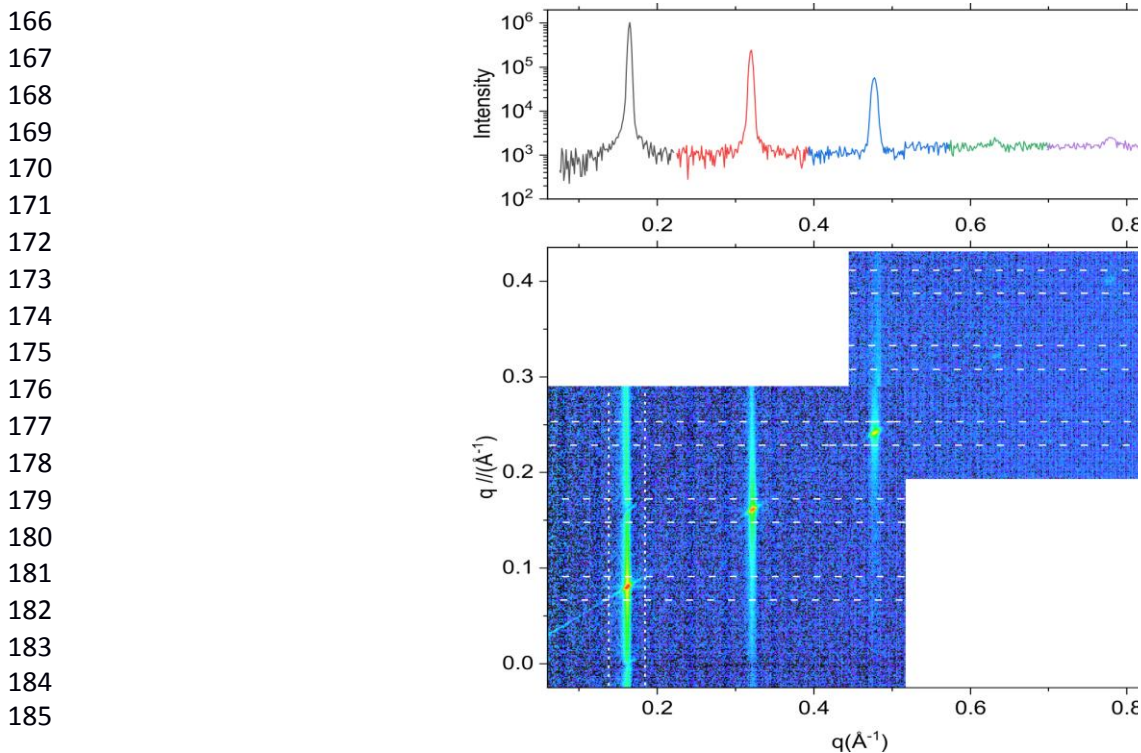
127 Neutron diffraction experiments were performed at the D16 neutron diffractometer [27] at the
 128 Institut Laue - Langevin (ILL, Grenoble, France). The incident wavelength was 4.46 \AA . The
 129 position sensitive Millimeter resolution Large Area Neutron Detector (MiLAND, 320 x 320
 130 mm^2 with 1 x 1 mm pixel resolution) was set to a sample-to-detector distance of 950 mm.
 131 Sample rocking scans (Ω -scans) were used to collect neutron diffraction data in reflection
 132 geometry by scanning the sample angle with respect to the incident beam (Ω) using 0.05 $^\circ$
 133 increments at two detector angles Γ relative to the incident neutron beam, $\Gamma = 12^\circ$ ($-1 < \Omega <$
 134 12°) and $\Gamma = 28^\circ$ ($8 < \Omega < 18^\circ$) in order to collect the maximum number of diffraction orders
 135 (Figure 2). The resulting q-range investigated was $q = 0.06 \text{ \AA}^{-1} - 0.86 \text{ \AA}^{-1}$, where q is the
 136 neutron scattering vector. Diffraction experiments were performed using a set of three
 137 identical [28] humidity chambers (BerILL) developed at ILL, allowing for precise control of
 138 the humidity and the temperature. The temperature at the sample position was kept at the
 139 constant value of $T = 25^\circ\text{C}$. The relative humidity (RH) was precisely regulated by the
 140 temperature difference between the sample and the water reservoir controlled independently

141 using a dedicated controller for the chambers and a Lakeshore 336 (Lake Shore Cryotronics,
142 Inc., Westerville, OH, USA) for the readout of the high-precision temperature sensors [28].

143 The DCPC samples, pure or containing 4% of either hydrogenated or deuterated alkanes,
144 were measured following two different procedures. In the first (*contrast variation*
145 *experiments*), samples were incubated at a constant RH of 97% for 2 hours before starting
146 each scan. Every sample was incubated three times inside the humidity chamber at different
147 D_2O contrasts, with the reservoir filled with 20 ml of different mixtures of D_2O/H_2O (8%, 70%
148 or 100%). The different contrasts were used to extract the phase of each Bragg reflection
149 required to determine the membrane neutron scattering length density (NSLD) profile [8].

150 In the second experimental procedure (*swelling experiments*), the D_2O/H_2O solvent contrast
151 was set to a zero NSLD obtained using the 8% D_2O mixture. Here, the RH was varied from
152 30% up to $\approx 100\%$ in order to scan the sample lamellar periodicity and Bragg reflection
153 intensities as a function of humidity from a dehydrated state up to full hydration. Sample
154 equilibration was gradually increased from 1 hour (used for the lowest humidity steps) up to
155 2.5 hours for the sample equilibrated at 99.5% RH. For the last measurement aimed at
156 reaching full hydration, samples were equilibrated offline for 24 hours in the measurement
157 chamber.

158 An example of reciprocal space map obtained by merging two Ω -scans is shown in Figure 2.
159 The first visible feature is the occurrence of a series of reflections located at the same
160 periodicity (q_z) on top of the line $q_{||} = (q)/2$ that corresponds to the specular condition. The
161 periodicity identified by the reflections results from the lamellar ordering of the multilayer,
162 with a repeat or center-to-center distance given by one bilayer plus one water layer. Each
163 reflection does not have the shape of a Bragg peak as expected from a perfect crystal, but
164 that of a Bragg sheet in the vertical ($q_{||}$) direction, due to fluctuations and defects in the liquid
165 crystal's organization.



186
187 **Figure 2.** Example of reciprocal space map ($q_{||}$ vs q) of DCPC at 8% D_2O contrast and 30% relative
188 humidity showing 5 lamellar diffraction orders. Horizontal white dashed lines show the limits of

189 integration for each diffraction order, while the top plot shows the result of the integrations truncated in
190 the selected Ω and 2θ regions of interest for the peak fitting.

191 These elongated features are a sign of the disorder both static or dynamic of the membrane
192 stack. Two minima lines can be observed from the 2D map, one that is located at constant Ω
193 = 0 and the other tracing the line $\Omega = 2\theta$. These minima correspond to the so-called *sample*
194 *horizons*, and occur at the angles where the scattered beam is attenuated by crossing
195 longitudinally the lamellar stack on the silicon substrate.

196 1. Data reduction

197 Data reduction was performed using the ILL software LAMP [29]. Pixel efficiency as well as
198 solid angle corrections were performed using a detector calibration obtained from the flat
199 incoherent scattering signal of a water measurement. The background was obtained by
200 collecting an empty humidity chamber scan and was subtracted from each measurement.
201 The background-subtracted data were then exported for further analysis using Origin Pro
202 (Version 2019, OriginLab Corporation, Northampton, MA, USA). The data were reduced to
203 1D intensities vs 2θ plots by integrating for each peak a slice of $\Omega = 1^\circ$ width around the
204 peak center (see Figure 2).

205 The integrated intensities of the Bragg peaks were obtained using Gaussian fits, as done
206 previously [30]. The angle (θ) of a Bragg peak is related to the scattering vector (q) by:

$$207 \quad q = \frac{4\pi\sin(\theta)}{\lambda} \quad (1)$$

208 where λ is the wavelength of the incident neutron beam. The periodicity (*d-spacing*) was
209 derived as in references [31, 32]. For each sample and experimental condition, a weighted
210 linear fit was performed on a plot of peak positions (in q) as a function of the diffraction order
211 (h) (known as *Bragg plot*), the slope (s) of which was used to determine the *d-spacing* via
212 the equation:

$$213 \quad d = \frac{2\pi}{s}. \quad (2)$$

214 The error on the *d-spacing* was obtained by propagating the error of the peak position fitting
215 and used in the weighted linear fit to the peak positions vs. Bragg order h .

216 The next step in the data analysis is to convert reciprocal space data into real space 1D
217 structures. For that, the calculated area of each peak was employed to construct neutron
218 scattering length density (NSLD) profiles from the sum of the neutron scattering lengths per
219 unit volume [33]. The way the membrane stack NSLD profiles can be constructed comes
220 from the definition of the scattering intensity $I(q)$ as:

$$221 \quad I(q) = P(q) * S(q) \quad (3)$$

222 where $P(q)$, the membrane form factor, contains information about the repeat unit structure
223 (in our case, one bilayer and one water layer) while $S(q)$, the structure factor, is related to
224 the spatial correlation between adjacent membranes that results from their interactions and
225 leads to the lamellar periodicity and to the Bragg reflections. Therefore, the $S(q)$ features
226 (the Bragg peaks) are modulated by the underlying form factor, and this property can be
227 used to sample the form factor dependence with q at discrete positions exploiting the
228 intensity modulation of all Bragg reflections that are observed in a sample scan [7-9]. The
229 Fourier transform of $P(q)$ in real space provides the NSLD profiles.

230 In practice, since one only has access to a finite number of q positions through the Bragg
231 reflections, approximated NSLD profiles are calculated from the discrete set of Fourier

232 coefficients F_h (also referred as “structure factors” in the text) using the following equation [7,
233 8, 10]:

$$234 \quad \rho(z) = \sum_{h=1}^{h_{max}} |F_h| v_h \cos\left(\frac{2\pi h}{d} z\right) \quad (4)$$

235 where d is the lamellar periodicity of the bilayer stack in the z direction perpendicular to the
236 membrane plane, $|F_h| = \pm\sqrt{I_h h}$ where I_h is the integrated intensity of the h^{th} order Bragg
237 peak and v_h is the phase of the structure factor terms that are in general complex quantities
238 including information on absorption and activation of the sample [34]. However, in the case
239 of centrosymmetric structures such as bilayers, $v_h = \pm 1$ and the phase assignment
240 simplifies into the assignment of a + or - sign for each F_h term [8].

241 Finally, from the data acquired by scanning the RH (swelling experiments), the osmotic
242 pressure (Π) [35, 36] could be calculated from the relative humidity using the following
243 equation:

$$244 \quad \Pi = \frac{-k_B T}{v_w^0} \ln(RH) \quad (5)$$

245 where RH is defined as P/P_0 (e.g. 0.5 for 50% RH), k_B is Boltzmann’s constant, T is the
246 temperature in Kelvin, and v_w^0 is the molecular volume of water [31].

247 2. Scattering Length Density profile determination

248 In order to gather insights about the membrane structural changes, the first step was to
249 extract the corresponding NSLD profiles of each sample. This was done by exploiting the
250 modulation in the intensity of each membrane Structure Factor term $F_h(q)$ as detailed in the
251 “Data reduction” section. The main challenge relies in the assignment of the phase which, in
252 the case of centrosymmetric structures such as membrane stacks, simplifies into the
253 assignment of a positive or negative sign to each term. In this work, we combined three
254 strategies to obtain an unambiguous phase assignment:

- 255 1. Contrast variation: the use of different D_2O / H_2O isotopic compositions allows to vary
256 the water NSLD that is the contrast between bilayers and water layers. By using the
257 fact that the NSLD of water increases linearly with the D_2O percentage, one can
258 detect the occurrence of phase changes.
259
- 260 2. Swelling: when the RH of the environment increases, the membrane stack
261 undergoes swelling, as a result of the hydration and the increase of the water layer
262 thickness. Assuming that the bilayer structure does not change when the water layer
263 increases, one can perform Relative Humidity (RH) scans and use the displacement
264 in q of the Bragg reflections to sample the $P(q)$ in a finite set of q positions [8]. With
265 this technique, one obtains information on the possible sign swapping whenever the
266 tracing of the $P(q)$ vs q highlights the presence of a relative minimum.
267
- 268 3. Physical considerations from the observed NSLD profiles: as highlighted in the
269 former points, the contrast variation and swelling techniques both allow detection of
270 phase changes, but not the absolute phases. However, the features of the NSLD
271 profiles can be qualitatively judged from our knowledge of the system. For instance,
272 the acyl chains placed in the middle of the bilayer should give a broad minimum in
273 the profile because of the high density of low scattering length hydrogen atoms.
274 Conversely, the phosphate groups of the phosphatidylcholines (the DCPC

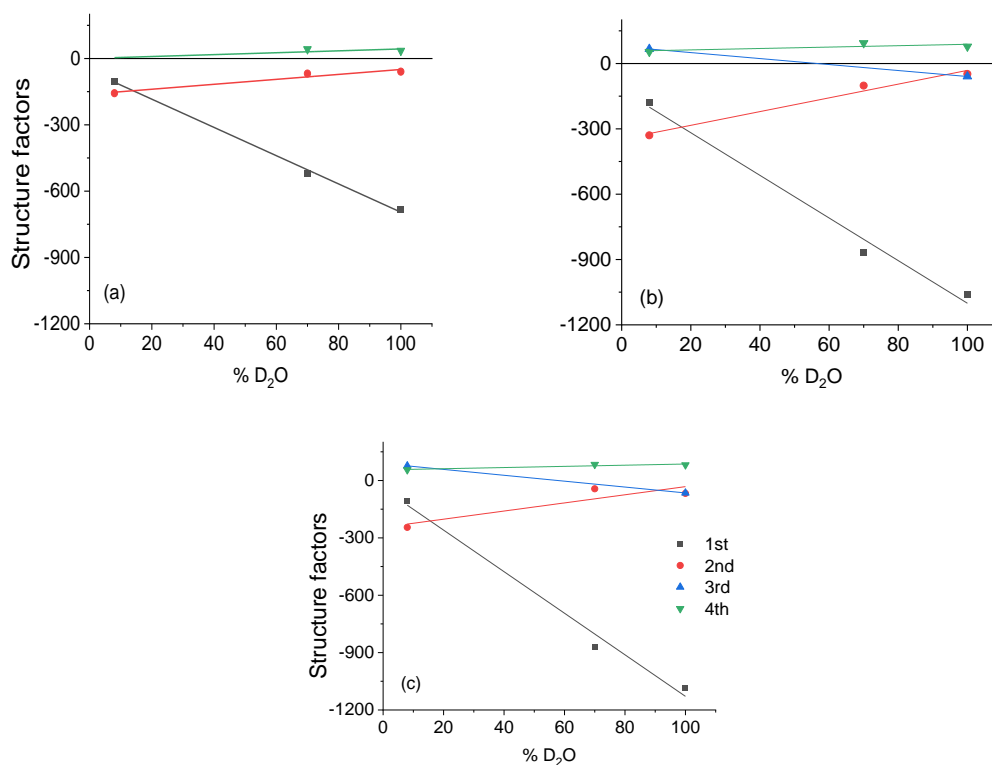
275 headgroups) give local maxima that will be highly visible at the lowest water contrast
276 of 8% D₂O. In addition, different D₂O contrasts at a constant RH do not change the
277 shape of the NSLD in the hydrocarbon region. Similar considerations were also made
278 when applying scaling and offset factors to the NSLD profiles to allow for
279 comparisons between different samples: there, the NSLD profiles of the different
280 samples were matched with each other in the solvent region, for the measurements
281 performed at the same D₂O / H₂O contrast.

282 Results

283 Figure 3 shows examples of the resulting contrast variation plots for the DCPC samples with
284 and without perdeuterated eicosane or squalane molecules. All numerical values of the
285 structure factor terms and the measured d-spacing can be found in Table 1 in the Electronic
286 Supplementary Information (ESI).

287 The choice of the sign for the 1st reflection order, the term which is a function of the overall
288 periodicity of the repeat unit (the d-spacing), is assigned as negative in order to obtain a
289 local minimum of the NSLD profiles at the z = 0 position (Figure 4). This translates into the
290 choice of setting the centre of the bilayer repeat unit at the 0 of the x-axis. All other phases
291 were assigned by making sure that, in the following order:

- 292 1) the linearity in the contrast variation plots was maintained (Figure 3);
- 293 2) combining the shape observation of the NSLD profiles at all 3 contrasts;
- 294 3) applying the phase change when needed (in our case, for the 3rd Bragg reflection order
295 around 70% D₂O/H₂O, visible in Figure 3).



296

297

298 **Figure 3.** Examples of contrast variation plots for the DCPC samples with and without added
299 alkanes. (a) DCPC. (b) DCPC + 4% d-eicosane. (c) DCPC + 4% d-squalane.

300

301

302

303

304

305

306

307

308

309

310

311

312

313

314

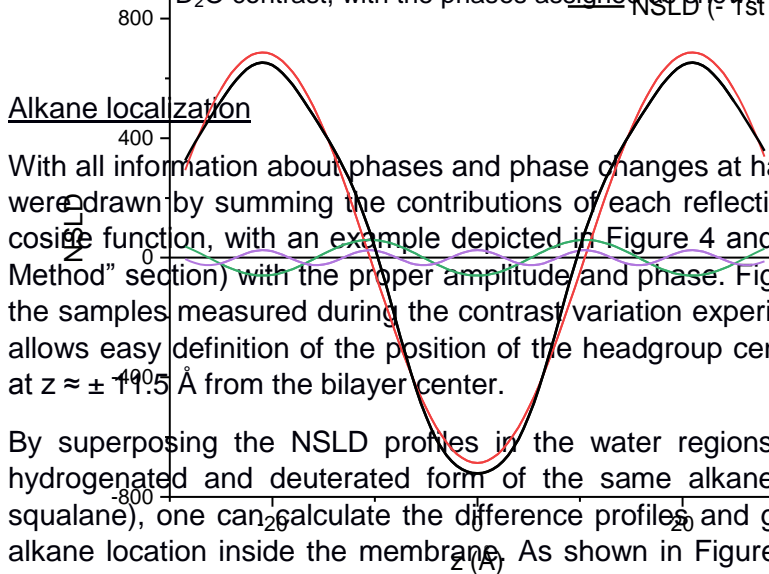
315

316

317

318

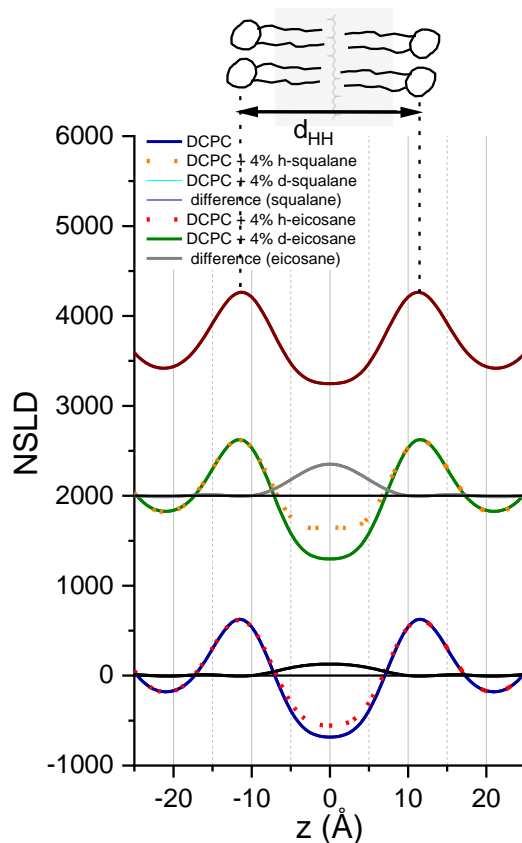
Figure 4. Plot of individual terms that contribute to the NSLD profile of the DCPC sample at 100% D₂O contrast, with the phases assigned as shown in panel (a) of Figure 3.



Alkane localization

With all information about phases and phase changes at hand, the membrane NSLD profiles were drawn by summing the contributions of each reflection order (all having the form of a cosine function, with an example depicted in Figure 4 and as detailed in the “Materials and Method” section) with the proper amplitude and phase. Figure 5 shows the NSLD profiles of the samples measured during the contrast variation experiments at 8% D₂O/H₂O contrast. It allows easy definition of the position of the headgroup centres, at the local maxima located at $z \approx \pm 11.5$ Å from the bilayer center.

By superposing the NSLD profiles in the water regions for the samples containing the hydrogenated and deuterated form of the same alkane (h- and d-eicosane; h- and d-squalane), one can calculate the difference profiles and get information about the average alkane location inside the membrane. As shown in Figure 5, both alkanes are found to be incorporated and sit inside the bilayer in the hydrocarbon region, preferentially in the midplane in between the monolayers.



319

320

321

322

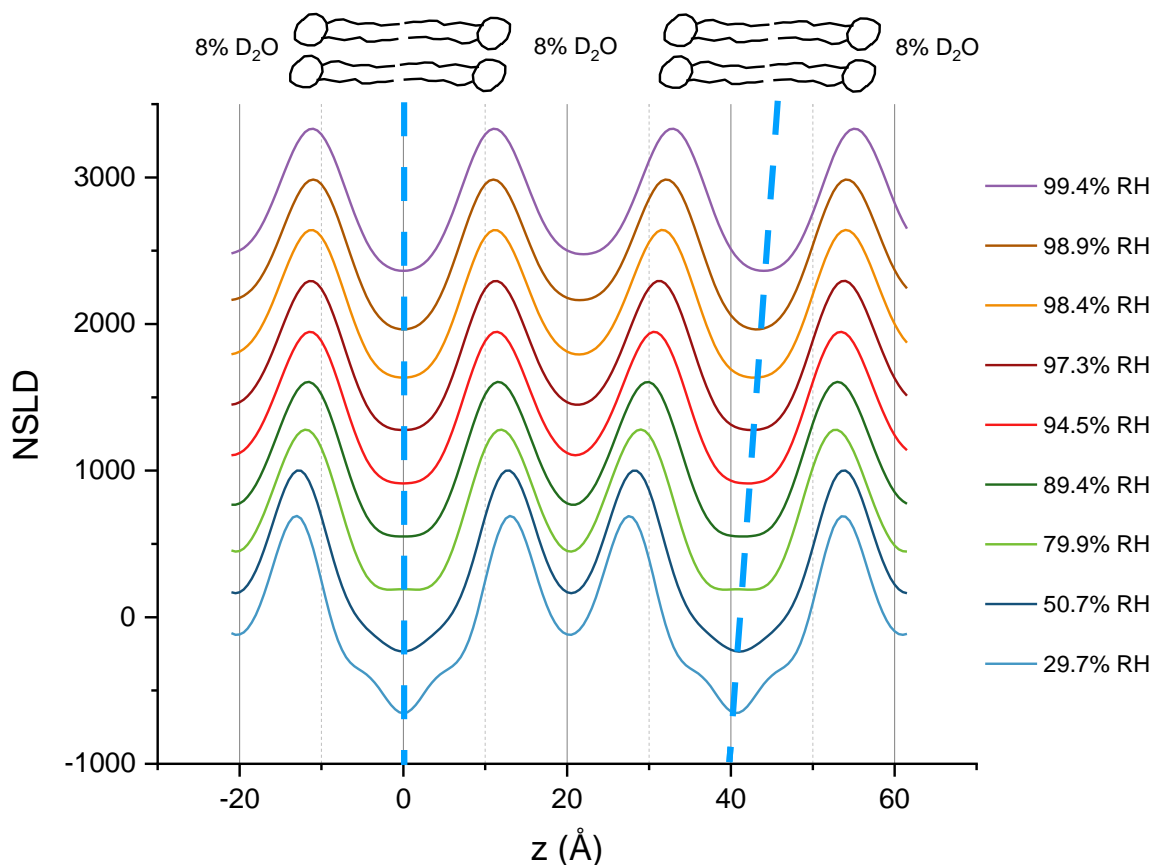
323

Figure 5. NSLD profiles at 8% D₂O contrast of samples measured at 97% RH. The y-axis scale refers to the alkane containing samples, while the other NSLD profiles were shifted for clarity. The top image shows a sketch of the bilayer with a molecule of squalane in the mid-plane, as mapped by the NSLD profiles within the dotted lines defined by d_{HH} the position of the maxima.

324 Membrane swelling

325 In addition to screening the phase of the membrane structure factors as a function of
326 humidity, swelling experiments (at 8% D₂O contrast, to easily locate the lipid headgroup
327 position) provided further information on the membrane characteristics and properties. The
328 samples measured here were a) DCPC; b) DCPC + 4% h-eicosane; c) DCPC + 4% h-
329 squalane; d) DCPC + 4% h-triacontane. All numerical values of the structure factor terms
330 can be found in Table 2 in the ESI. Figure 6 shows an example of the NSLD profiles
331 obtained at each measured RH for the DCPC sample. Some qualitative features are visible
332 from the plot:

- 333 - The lowest humidity values of 30% and 50% show a more pronounced minimum in
334 the centre of the bilayer. This can be attributed to the higher density of hydrogen
335 atoms at the terminal methyl group position, a feature that disappears at higher
336 humidity values presumably because of an increase in membrane static and/or
337 dynamic disorder.
- 338 - The repeat distance (d-spacing) increases with increasing RH, as expected because
339 of the water layer thickening between bilayers.
- 340 - The bilayer thickness decreases with increasing RH, shown in the plot as a shift of
341 the headgroup maxima position.



342
343 **Figure 6.** NSLD profiles of a DCPC sample during swelling experiments showing 2 unit cells. The
344 blue dotted lines show a perfect vertical line as reference on the left side and the effect of swelling
345 with a minimum shifted more and more to the right side. Top image represents the location of the two
346 bilayers mapped by the NSLD profiles. Water contrast was 8% D₂O.

347 The last two features can be used for quantitative comparison between the different samples
348 investigated. Figure S1 in the ESI shows the bilayer thickness changes as a function of
349 humidity for all samples. We use here the same nomenclature applied in former diffraction
350 studies carried out on DLPC and DMPC samples [12]. As a first definition of the bilayer
351 thickness, we define d_{HH} as the distance between the two maxima in the NSLD profiles at
352 8% D_2O contrast, that corresponds to the distance between the phosphate groups of the PC.

353 As shown in figure S1, d_{HH} decreases for all samples when humidity increases. Interestingly,
354 the membrane thickness of the samples containing eicosane and squalane appears to be
355 offset by a value of approximately $[0.5 - 1] \text{ \AA}$, while this is not observed for the sample
356 containing triacontane. The lipid molecular volume (V) being constant, the decrease in
357 bilayer thickness ($d_{HH} = 2l$ where l is the lipid length), is consistent with an increase of the
358 area per headgroup (A) upon increasing hydration, according to:

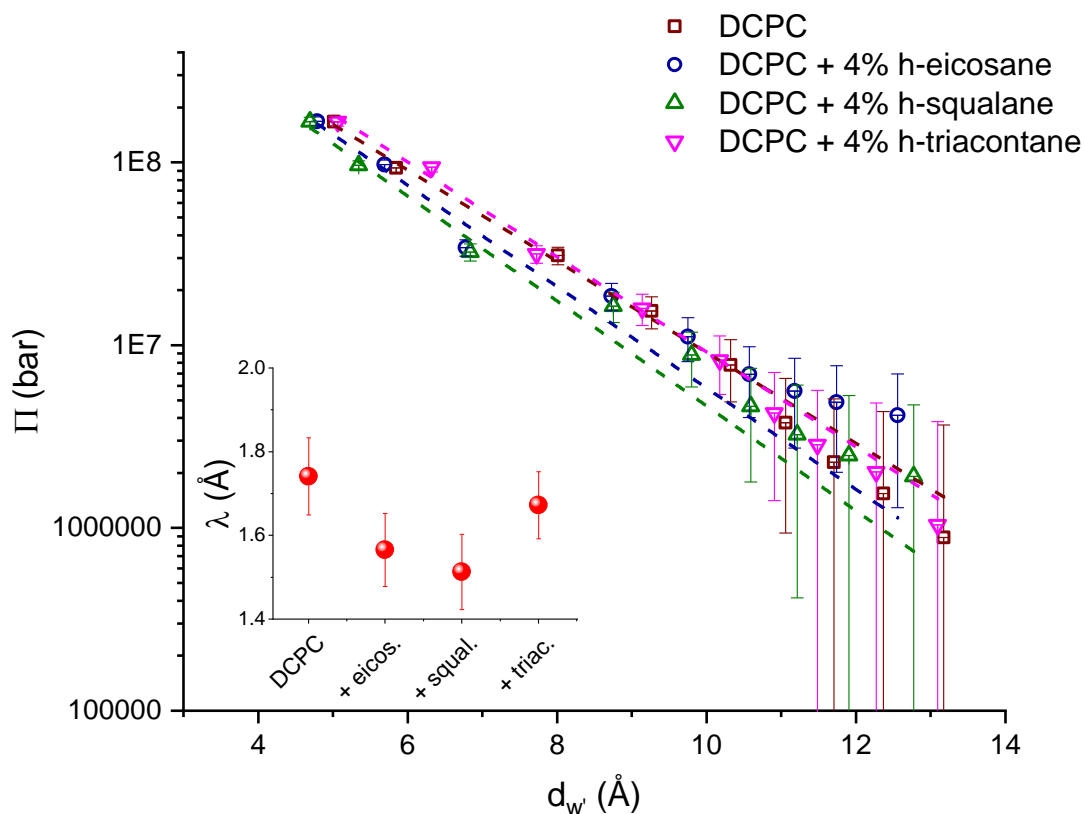
$$359 \quad A = \frac{V}{l}. \quad (6)$$

360 From previous data on DMPC and DLPC [12], since the headgroup area should not change
361 significantly between DMPC, DLPC and DCPC, we assume an average area $A \approx 62 \text{ \AA}^2$
362 between the reported values [12] $A = 60.6 \text{ \AA}^2$ (DMPC) and 63.2 \AA^2 (DLPC). Also,
363 considering the lipid volume V_L scaling linearly with the chain length ($V_L = 1101$ and 991 \AA^3
364 for DMPC and DLPC, respectively), we obtain $V_L \approx 881 \text{ \AA}^3$ and a calculated $d_{HH} \approx 20.3 \text{ \AA}$ for
365 DCPC at full hydration. As our reported value at maximum hydration is $d_{HH} \approx 22.5 \pm 0.5 \text{ \AA}$,
366 this result suggests that the DCPC membranes at the highest measured RH were close to
367 full hydration, but not fully hydrated, (Figure S1).

368 The feature of interest, namely the water layer thickness as a function of humidity, is shown
369 in the more common pressure – distance plot in Figure 7. In order to estimate the water layer
370 thickness d_w , we used existing data from the literature on PC lipids to estimate the thickness
371 of the headgroups [12]. This led to the following formula for our calculation of d_w :

$$372 \quad d_w = d - d_{b'} = d - d_{HH} - 8.1 \text{ \AA}. \quad (6)$$

373 where $d_{b'}$ is the bilayer thickness calculated from the interfaces water-headgroup.



374

375 **Figure 7.** Pressure-distance curves: osmotic pressure Π as a function of the water layer thickness d_w
 376 calculated for all samples. Inset: decay lengths found from exponential fits for the four samples.

377 The data show very small qualitative differences probably due to the humidity range
 378 explored, still far away from the expected values for maximum swelling in bulk with excess
 379 water (the water layer thickness at full swelling for PC lipids is known to be at $d_w \approx 20\text{-}22 \text{ \AA}$
 380 [12] and the bilayer thickness did not shrink to the expected minimum value, as previously
 381 reported). Exponential fits of Π as a function of d_w yield an estimation of the decay length λ
 382 (inset of Figure 7). Although the differences are small, the samples containing eicosane and
 383 squalane show slightly lower decay lengths which could imply a lower swelling limit for these
 384 two samples. The obtained λ values are slightly lower than the value reported in the
 385 literature for DLPC membranes (around $\lambda = 2.1 \text{ \AA}$) [37].

386 Discussion

387 Our results allow us to gain numerous insights regarding the structure of a short chain
 388 membrane model, with and without insertion of additional apolar molecules (linear and
 389 branched alkanes).

390 First, contrast variation measurements clearly show that both the alkanes, eicosane and
 391 squalane, are included in the hydrocarbon region of the DCPC bilayer (Figure 5). Compared
 392 to earlier studies by Hauss et al. [18] and Salvador-Castell et al. [38], we find an alkane layer
 393 of almost identical size, so that we can conclude that the alkanes are likely oriented
 394 perpendicular to the lipid acyl chains. In addition, the bilayer thickness values calculated
 395 from fitting the maxima of the NSLD profiles at 8% D_2O contrast (Figure S1) show an offset
 396 of $\approx 0.5 - 1 \text{ \AA}$ compared to the alkane-free DCPC membrane, confirming further the
 397 incorporation of the alkanes in the mid-plane.

398 Such finding is of primary importance for the protomembrane model suggested here. A
 399 similar strategy was forwarded already for modern membranes in archaeal cells, which

400 withstand the most extreme conditions. We found a similar architecture and investigated in
401 many details the consequences of the presence of the apolar lipids [19, 38]. In particular,
402 they are able to extend the stability domain, to reduce the membrane's permeability to
403 protons but to increase that of water, and to induce a negative curvature in the membrane,
404 allowing the transition to novel non-lamellar phases. As these characteristics are mandatory
405 for the good functioning of the membrane in extreme conditions, they can be taken as
406 indicative for the architecture of protomembranes, and we found already positive impact of
407 alkanes on the stability of protomembranes under high temperature and pressure conditions
408 [39, 40] and on their molecular dynamics [41]. In this context the experimental proof of the
409 presence of the apolar lipids is an important step.

410 Interestingly, a slight increase of the bilayer thickness offset with humidity increase
411 (differences in Figure S1) might suggest a small effect of the hydration in increasing the
412 portion of alkane molecules accommodating in the mid-plane normal to the bilayer plane.
413 The thickness offset is not observed on the sample containing triacontane, which suggests
414 that it is not included in the bilayer and that size might play a role in the ability of such
415 molecules to be successfully inserted within the bilayer. The long-axis length of eicosane
416 (C20) and squalane (C30) being similar (because of the branched structure of the squalane)
417 and of the same order of twice the lipid chain length of DCPC are capable of inserting within
418 the membrane, however the triacontane size could not be accommodated in the
419 hydrocarbon region by intercalating parallel to the lipid chains (see Figure 1). Perhaps due to
420 the need for the membrane to assume a certain undulated in-plane arrangement (governed
421 by the lipid intrinsic geometry and the membrane bending/compression moduli), the
422 arrangement of triacontane perpendicular to the lipid chain is not possible, so that these
423 molecules are excluded from the membrane and are not observed in the calculated NSLD
424 profiles. Such a conclusion remains, however, speculative.

425 All membrane stacks investigated show a clear effect of the humidity increase in thinning the
426 bilayer up to ≈ 4 Å in the humidity range $\approx 30 - 100\%$, which is consistent with the increase
427 of the headgroup area observed in PC lipids of longer chain lengths [12]. The extent of such
428 decrease in bilayer thickness is not affected by the inclusion of alkane molecules. The decay
429 length of the samples containing eicosane and squalane is slightly lower than that of
430 pure DCPC, implying a possible lower swelling limit induced by the alkane presence. The
431 compatible value of λ between DCPC and DCPC + triacontane samples gives an additional
432 indication that the latter alkane did not incorporate into the membrane.

433 To summarize, we have performed an extensive study of DCPC oriented membrane stacks
434 as a function of the relative humidity (RH) and at different D_2O/H_2O contrasts. This allowed
435 us to determine the bilayer NSLD profile and to define unambiguously the phase of each of
436 the structure factor terms F_h .

437 From that, and by using deuterium labelled alkanes, we found that eicosane and squalane
438 are inserted inside the model membrane in the hydrocarbon region. At least a significant
439 portion of the alkane molecules inserts perpendicular to the lipid chains, causing a small but
440 significant increase in the bilayer thickness d_b , consistent with a confined elongated position
441 of the compound in the mid-plane. The membrane swelling induced by the increase in
442 humidity causes, on one hand, an increase of the intermembrane water thickness (as
443 expected), while on the other hand it leads to a slight decrease in the bilayer thickness,
444 which can be explained by a concomitant volume increase of the lipid headgroup upon
445 hydration. The decrease of d_{HH} is not affected by the eicosane or squalane presence inside
446 the membrane.

447 The sample containing the longer linear hydrocarbon alkane triacontane does not show any
448 increase in the bilayer thickness. This, together with physical considerations about the
449 alkane and lipid molecule sizes, implies that the triacontane molecules do not incorporate
450 into the membrane, unlike eicosane and squalane. This is consistent with the selective
451 exclusion of triacontane (and inclusion of squalane) molecules that has been reported in a
452 former study with different membrane compositions [19]. The slight differences in osmotic
453 pressure decay with water thickness d_w indicate that the eicosane and squalane may
454 decrease the membrane maximum swelling limit of the membrane.

455 Therefore, the incorporation of certain alkanes within short chain lipid membranes could
456 have also occurred in an origin of life scenario, where both these alkanes and membrane-
457 forming SCA could have been synthesized abiotically. This membrane enrichment, coupled
458 with the existence of a preferential structural arrangement of the n-alkanes in the
459 hydrophobic core, can effectively increase the membrane thickness and possibly lead to a
460 lower membrane swelling capability. Together with previously observed effects in increasing
461 the membrane thermal and pressure stability [21], the results suggest a role of the n-alkanes
462 in modifying significantly the membrane structural and functional properties, constituting one
463 of the possible survival strategies against the extreme prebiotic environmental conditions for
464 the first membrane compartments at the origin of life.

465 **Acknowledgements**

466 LM was supported by a scholarship from the Institut Laue - Langevin (ILL) PhD program.
467 The authors thank ILL for neutron beamtime on D16 (DOI: 10.5291/ILL-DATA.9-13-758 and
468 10.5291/ILL-DATA.9-13-906). The ILL Partnership for Soft Condensed Matter (PSCM) is
469 acknowledged for the access to the lab infrastructures.

470 **References**

471

472

- 473 [1] J.W. Szostak, D.P. Bartel, P.L. Luisi, Synthesizing life, *Nature*, 409 (2001) 387-390.
474 [2] D. Segre, D. Ben-Eli, D.W. Deamer, D. Lancet, The lipid world, *Orig Life Evol Biosph*, 31 (2001) 119-
475 145.
476 [3] P.L. Luisi, P. Walde, T. Oberholzer, Lipid vesicles as possible intermediates in the origin of life,
477 *Curr. Opin. Coll. Inter. Sci.*, 4 (1999) 33 - 39.
478 [4] D. Deamer, The Role of Lipid Membranes in Life's Origin, *Life (Basel)*, 7 (2017).
479 [5] M. Fiore, P. Strazewski, Prebiotic Lipidic Amphiphiles and Condensing Agents on the Early Earth,
480 *Life (Basel)*, 6 (2016).
481 [6] O.G. Mouritsen, *Life - As a Matter of Fat*, The Frontiers Collection, Place Published, 2005.
482 [7] G. Zaccai, J.K. Blasie, B.P. Schoenborn, Neutron diffraction studies on the location of water in
483 lecithin bilayer model membranes, *Proc Natl Acad Sci U S A*, 72 (1975) 376-380.
484 [8] D.L. Worcester, N.P. Franks, Structural analysis of hydrated egg lecithin and cholesterol bilayers II.
485 Neutron diffraction, *J. Mol. Biol.*, 3 (1976) 359 - 378.
486 [9] N.P. Franks, W.R. Lieb, The structure of lipid bilayers and the effects of general anaesthetics: an x-
487 ray and neutron diffraction study, *J. Mol. Biol.*, 134 (1979) 469 - 500.
488 [10] G. Büldt, H.U. Gally, J. Seelig, G. Zaccai, Neutron diffraction studies on phosphatidylcholine
489 model membranes: I. Head group conformation, *J. Mol. Biol.*, 134 (1979) 673 - 691.
490 [11] J.F. Nagle, S. Tristram-Nagle, Structure of lipid bilayers, *Biochim Biophys Acta*, 1469 (2000) 159-
491 195.

492 [12] N. Kucerka, Y. Liu, N. Chu, H.I. Petrache, S. Tristram-Nagle, J.F. Nagle, Structure of Fully Hydrated
493 Fluid Phase DMPC and DLPC Lipid Bilayers Using X-Ray Scattering from Oriented Multilamellar Arrays
494 and from Unilamellar Vesicles, *Biophys. J.*, 88 (2005) 2626-2637.

495 [13] N. Kucerka, S. Tristram-Nagle, J.F. Nagle, Structure of Fully Hydrated Fluid Phase Lipid Bilayers
496 with Monounsaturated Chains, *J. Membr. Biol.*, 208 (2006) 193 - 202.

497 [14] D.A. Haydon, B.M. Hendry, S.R. Levinson, J. Requena, Anaesthesia by the n-alkanes. A
498 comparative study of nerve impulse blockage and the properties of black lipid bilayer membranes,
499 *BBA - Biomembranes*, 470 (1977) 17 - 34.

500 [15] D.A. Haydon, B.M. Hendry, S.R. Levinson, J. Requena, The molecular mechanisms of
501 anaesthesia, *Nature*, 268 (1977) 356 - 358.

502 [16] S.H. White, G.I. King, J.E. Cain, Location of hexane in lipid bilayers determined by neutron
503 diffraction, *Nature*, 290 (1981) 161 - 163.

504 [17] T.J. McIntosh, S.A. Simon, R.C. MacDonald, The organization of n-alkanes in lipid bilayers, *BBA -*
505 *Biomembranes*, 597 (1980) 445 - 463.

506 [18] T. Hauss, S. Dante, N.A. Dencher, T.H. Haines, Squalane is in the midplane of the lipid bilayer:
507 implications for its function as a proton permeability barrier, *BBA - Bioenergetics*, 1556 (2002) 149 -
508 154.

509 [19] M. Salvador-Castell, B. Deme, P. Oger, J. Peters, Lipid Phase Separation Induced by the Apolar
510 Polyisoprenoid Squalane Demonstrates Its Role in Membrane Domain Formation in Archaeal
511 Membranes, *Langmuir*, 36 (2020) 7375-7382.

512 [20] A. Cario, V. Grossi, P. Schaeffer, P.M. Oger, Membrane homeoviscous adaptation in the piezo-
513 hyperthermophilic archaeon *Thermococcus barophilus*, *Frontiers in Microbiology*, 6 (2015).

514 [21] L. Misuraca, B. Demé, P. Oger, J. Peters, Alkanes increase the stability of early life membrane
515 models under extreme pressure and temperature conditions, *Communications Chemistry*, 4 (2021)
516 24, 21 - 28.

517 [22] T.M. McCollom, G. Ritter, B.R. Simoneit, Lipid synthesis under hydrothermal conditions by
518 Fischer-Tropsch-type reactions, *Orig Life Evol Biosph*, 29 (1999) 153-166.

519 [23] B.R.T. Simoneit, Prebiotic organic synthesis under hydrothermal conditions: an overview,
520 *Advances in Space Research*, 33 (2004) 88 - 94.

521 [24] N. Kucerka, M.P. Nieh, J. Katsaras, Fluid phase lipid areas and bilayer thicknesses of commonly
522 used phosphatidylcholines as a function of temperature, *Biochim Biophys Acta*, 1808 (2011) 2761-
523 2771.

524 [25] L. Misuraca, A. Calio, I. Grillo, A. Grelard, P.M. Oger, J. Peters, B. Demé, High-Temperature
525 Behavior of Early Life Membrane Models, *Langmuir*, 36 (2020) 13516-13526.

526 [26] S. Tristram-Nagle, R. Zhang, R.M. Suter, C.R. Worthington, W.J. Sun, J.F. Nagle, Measurement of
527 chain tilt angle in fully hydrated bilayers of gel phase lecithins, *Biophys J*, 64 (1993) 1097-1109.

528 [27] V. Cristiglio, B. Giroud, L. Didier, B. Demé, D16 is back to business: More neutrons, more space,
529 more fun, *Neutron News*, 26 (2015) 22 - 24.

530 [28] J. Gonthier, M.A. Barrett, O. Aquettaz, S. Baudoin, E. Bourgeat-Lami, B. Demé, N. Grimm, T.
531 Hauss, K. Kiefer, E. Lelièvre-Berna, A. Perkins, D. Wallacher, BerILL: The ultimate humidity chamber
532 for neutron scattering, *J. Neutron Res.*, 21 (2019) 65 - 76.

533 [29] D. Richard, M. Ferrand, G.J. Kearley, Analysis and visualisation of neutron-scattering data,
534 *Journal of Neutron Research*, 4 (1996) 33-39.

535 [30] N. Kucerka, M.P. Nieh, J. Pencer, J.N. Sachs, J. Katsaras, What determines the thickness of a
536 biological membrane, *Gen Physiol Biophys*, 28 (2009) 117-125.

537 [31] M. Kanduc, A. Schlaich, A.H. de Vries, J. Jouhet, E. Marechal, B. Deme, R.R. Netz, E. Schneck,
538 Tight cohesion between glycolipid membranes results from balanced water-headgroup interactions,
539 *Nat Commun*, 8 (2017) 14899.

540 [32] A.R. Denninger, B. Deme, V. Cristiglio, G. LeDuc, W.B. Feller, D.A. Kirschner, Neutron scattering
541 from myelin revisited: bilayer asymmetry and water-exchange kinetics, *Acta Crystallogr D Biol*
542 *Crystallogr*, 70 (2014) 3198-3211.

543 [33] D. Marquardt, F.A. Heberle, J.D. Nickels, G. Pabst, J. Katsaras, On scattered waves and lipid
544 domains: detecting membrane rafts with X-rays and neutrons, *Soft Matter*, 11 (2015) 9055-9072.
545 [34] <https://www.ncnr.nist.gov/resources/activation/>
546 [35] D.M. LeNeveu, R.P. Rand, V.A. Parsegian, Measurement of forces between lecithin bilayers,
547 *Nature*, 259 (1976) 601-603.
548 [36] V.A. Parsegian, N. Fuller, R.P. Rand, Measured work of deformation and repulsion of lecithin
549 bilayers, *Proc. Natl. Acad. Sci. USA*, 76 (1979) 2750 - 2754.
550 [37] E. Sparr, H. Wennerstrom, Responding phospholipid membranes--interplay between hydration
551 and permeability, *Biophys J*, 81 (2001) 1014-1028.
552 [38] M. Salvador-Castell, M. Golub, N. Erwin, B. Demé, N.J. Brooks, R. Winter, J. Peters, P.M. Oger,
553 Characterisation of a synthetic Archeal membrane reveals a possible new adaptation route to
554 extreme conditions, *Commun Biol*, 4 (2021) 653.
555 [39] L. Misuraca, A. Calio, J.G. LoRicco, I. Hoffman, R. Winter, B. Demé, J. Peters, P.M. Oger, Alkanes
556 as membrane regulators of the response of early membranes to extreme temperatures, *Life*, (2022)
557 accepted for publication.
558 [40] L. Misuraca, A. Calio, J.G. LoRicco, I. Hoffman, R. Winter, B. Demé, J. Peters, P.M. Oger, Alkanes
559 as Membrane Regulators of the Response of Early Membranes to Extreme Temperatures, *life*, 12
560 (2022) 445, 441 - 447.
561 [41] L. Misuraca, T. Matsuo, A. Cisse, J. LoRicco, A. Calio, J.M. Zanotti, B. Deme, P. Oger, J. Peters,
562 High temperature molecular motions within a model protomembrane architecture, *Phys Chem*
563 *Chem Phys*, (2022).

564